

We are IntechOpen, the world's leading publisher of Open Access books Built by scientists, for scientists

6,900

Open access books available

186,000

International authors and editors

200M

Downloads

Our authors are among the

154

Countries delivered to

TOP 1%

most cited scientists

12.2%

Contributors from top 500 universities



WEB OF SCIENCE™

Selection of our books indexed in the Book Citation Index
in Web of Science™ Core Collection (BKCI)

Interested in publishing with us?
Contact book.department@intechopen.com

Numbers displayed above are based on latest data collected.
For more information visit www.intechopen.com



One-Dimensional Photonic Crystals With the Superconducting Defects

N. N. Dadoenkova, A. E. Zabolotin,
Yu. S. Dadoenkova, I. L. Lyubchanskii, Y.P. Lee and
Th. Rasing

Additional information is available at the end of the chapter

<http://dx.doi.org/10.5772/59971>

1. Introduction

During the last 27 years, starting from pioneering papers by E. Yablonovich [1] and S. John [2], photonic crystals (PCs) or photonic band gap (PBG) materials are the objects of intensive theoretical and experimental research, because of promising applications in modern photonics and related areas [3–6]. Usually, PCs are artificial one-, two- or three-dimensional (1D, 2D, and 3D) periodic structures with periods which are comparable with the wavelengths of electromagnetic waves (EMWs) and constructed of materials with different refractive indices [3–6]. The PBGs are forbidden regions in the dispersion law and in transmittivity spectra, where EMWs with selected frequencies cannot propagate through the PC. A lot of attention has been directed to the study of conventional PCs on the base of dielectrics, semiconductors, and normal metals as well as on the base of functional materials like magnetics [7, 8], ferroelectrics [9, 10] and liquid crystals [6, 11, 12] which can be controlled by external magnetic or electric fields. Another interesting group of PCs are those with superconducting (SC) constituents, so-called superconducting PCs. Scientific activity in different aspects of SC PC is described in several original and review papers by S. Savel'ev et al. [13 – 15], and in the review paper by S. Anlage [16]. The majority of papers about SC PC is devoted to regular periodic photonic structures. But, if the periodicity of a PC is destroyed by the introduction of a so-called defect unit, for example a defect layer into a 1D PC, the transmittivity spectra are drastically changed. In that case, defect modes (DMs) emerge inside the PBG because of localization of EMWs around the defect unit.

These DMs can be observed as very narrow peaks (in comparison with the PBG widths) with sufficiently large transmittivity. If such defects are made of functional materials which are sensitive to the action of various external factors like electric or magnetic fields or temperature, it is possible to control the transmittivity of PCs at the DM frequencies.

In our papers [17, 18] we investigated the influence of a complex defect layer constructed from dielectric and SC sublayers on the transmittivity of PCs for different thicknesses of the SC constituent and temperatures for normal [17] and oblique [18] incidence of EMWs on the PC.

In [19] it was shown that a thin SC layer on the top of a dielectric PC leads to selective transmittivity for different polarizations of incident EMWs. The influence of a complex defect layer (composed of SC and dielectric sublayers) as a spacer between two different PCs was studied in [20]. The localized modes in a metamaterial-dielectric PC with a dielectric-SC pair defect were investigated in [21]. The behavior of a DM inside a PBG depending on position (SC-dielectric and dielectric-SC) in a 1D PC was analyzed in [22]. In a recent paper [23], the normal and oblique incidence of an EMW on 1D dielectric PC with a thin SC defect layer was theoretically investigated and the obtained results show qualitative agreement with our calculations [17, 18]. An interesting situation takes place when two (or more) defects are introduced into a PC. In the case of two defects two DMs appear inside PBG and their mutual positions strongly depend on the distance between the defect units. The linear and nonlinear optical, as well as, magneto-optical properties of 1D PCs with two magnetic defects were theoretically studied in a few papers [24 – 27]. In these papers some interesting peculiarities of the spectra of DMs inside the PBGs, like the possibilities to obtain relatively wide peaks formed by two DMs, were obtained and discussed. One expect that in PCs with two complex defects composed of SC and dielectric sublayers one can obtain new peculiarities as well.

In this chapter, we theoretically investigate the transmittivity, reflectivity and absorptance of 1D PCs with one and two complex defects containing SC constituents. Two cases of asymmetric positions of complex SC-containing defects (when both SC-sublayers are located on the right-hand, or on the left-hand sides of the dielectric defect sublayers inside the photonic structure) are investigated, as well as the symmetric ones. We also analyze the dependencies of the optical properties of such PCs as functions of SC-sublayer thicknesses and temperature. The chapter is organized as follows. In Sec. 2 we describe the aforementioned photonic structure with one complex defect layer with an analytical approach. In Sec. 3 the numerical calculations of the transmittivity spectra for the photonic structure two superconducting defect layers are presented. In Sec. 4, conclusions, we summarize the obtained results.

2. Photonic crystal with one defect

Let us consider finite 1D periodic photonic structure composed of two finite size PCs of structure $(AB)^5$ with the period $D=d_1+d_2$, where the layer A is the strontium titanate $SrTiO_3$ with thickness d_1 , the layer B is the aluminum oxide Al_2O_3 with thickness d_2 , and the complex defect layer placed between these PCs, as shown in Fig. 1. We assume the medium surrounding the photonic structure to be a vacuum. The layers of PC are located in the xy -plane and the z -axis

to be normal to the interfaces. The defect layer consists of SC sublayer $YBa_2Cu_3O_7$ of thickness d_s and dielectric sublayer $SrTiO_3$ of thickness d_{1Def} , respectively. The selection of these dielectrics is due to the fact that both these materials $SrTiO_3$ and Al_2O_3 are widely used as substrates for $YBa_2Cu_3O_7$ SC films.

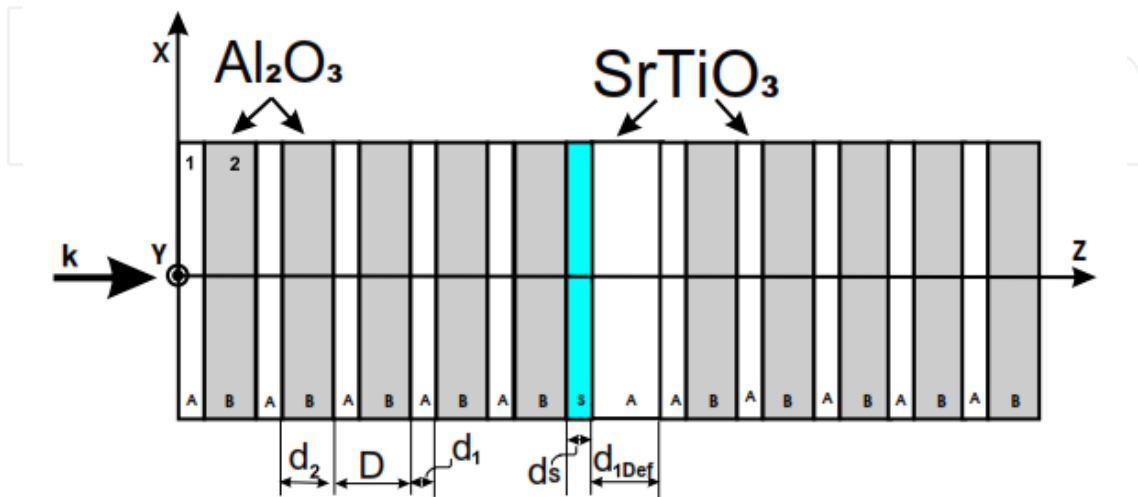


Figure 1. Schematic of photonic structure which is containing of two finite-size PCs with complex SC-dielectric defect: $(AB)^5(Sc)(defA)(AB)^5$.

For the SC layers, we consider the case when the crystallographic a -axis (electrically "light" axis) and c -axis (electrically "heavy" axis) of $YBa_2Cu_3O_7$ coincide with the x - and y -axes, respectively. In our study we used the frequency- and temperature-dependent dielectric permittivity tensor for $YBa_2Cu_3O_7$ with nonzero diagonal components $\epsilon_{xx}(\omega, T) = \epsilon_{zz}(\omega, T)$ and $\epsilon_{yy}(\omega, T)$, introduced in Ref. [19] on the base of a generalized two-fluid model in the following form:

$$\epsilon_{s,v}(\omega, T) = 1 + \frac{4\pi i}{\omega} \sigma_{s,v}(\omega, T), \quad v = xx, yy. \tag{1}$$

Here the dynamic electrical conductivity tensor $\sigma_{s,v}(\omega, T)$ is defined as

$$\sigma_{s,v}(\omega, T) = f_+(\omega, T) \sigma_{s,v}^+(\omega, T) + f_-(\omega, T) \sigma_{s,v}^-(\omega, T), \tag{2}$$

where $\sigma_{s,v}^+(\omega, T)$ are determined as follows:

$$\sigma_{s,v}^-(\omega, T) = \frac{T_c}{\Lambda_{s,v}^{(0)}(\alpha T - i\omega T_c)}, \quad \sigma_{s,v}^+(\omega, T) = \frac{i(T^4 - T_c^4)}{\omega \Lambda_{s,v}^{(0)} T_c^4} + \left[\frac{T}{T_c} \right]^4 \sigma_{s,v}^-(\omega, T), \tag{3}$$

where T_c and $f_{\pm}(\omega, T)$ are the critical temperature and the electron distribution functions, respectively,

$$f_{\pm}(\omega, T) = \left(1 + \exp\left(\frac{\pm \hbar(\omega - \omega_s(T))}{k_B T}\right) \right)^{-1}, \quad (4)$$

where k_B and \hbar are the Boltzmann's and Planck's constants, respectively. In Eq. (4) the pair breaking frequency ω_s is determined via the temperature-dependent superconductor half-gap energy $\Delta(T)$ as $\hbar\omega_s = \Delta(T)$, which is approximated as $\Delta(T) \cong \Delta_0 \left(1 - \frac{T^3}{T_c^3}\right)^{1/4}$ (see for details Ref. [19]).

In the optical and near infra-red regimes the electro-dynamical properties of $YBa_2Cu_3O_7$ can be described by a dielectric permittivity only. The magnetic permeability of $YBa_2Cu_3O_7$ is assumed to be $\mu_s = 1$.

It should be noted that SC sublayer exhibits strongly pronounced anisotropy of optical properties. Both components of the permittivity tensor $\varepsilon_{s,xx}$ and $\varepsilon_{s,yy}$ are complex values, moreover, in considered frequency region (first PGB) both real and imaginary parts of $\varepsilon_{s,xx}$ are about two order of magnitude larger than corresponding ones for $\varepsilon_{s,yy}$. As $\varepsilon_{s,yy}$ and $\varepsilon_{s,xx}$ are responsible for TE- and TM- polarized modes, respectively, it means that decaying of TM-polarized mode inside SC sublayer is much stronger than of TE-polarized one. This difference in values of $\varepsilon_{s,xx}$ and $\varepsilon_{s,yy}$ leads to drastic contrast in behavior TE- and TM- modes with variation of the SC sublayer thickness d_s .

We investigate the case of the normal incidence of light on the right hand surface of the PCs. We assume the incident light to be linearly polarized: x - or y - polarizations (the EMWs with electric field vector \mathbf{E} vibrations along the x - or y -axis, respectively).

We calculate the transmittivity and reflectivity spectra of the 1D PC using the four-dimensional transfer matrix method by Berreman [29]. The details of the method are given in our previous papers [17, 18, 30].

In the case of non-SC defect layer (single dielectric layer with thickness $d_{def} = d_1$) symmetrically embedded between two identical PCs, the dependence of transmittivity for both TE- and TM-modes in 1D PC is characterized by the presence of defect mode in the center of PBGs, as depicted on Fig. 2.

As shown in Ref. [19], a thin SC layer, deposited at one side of dielectric PC, leads to the decrease of transmittivity for the EMW, polarized along the x -axis (TM-mode), whereas TE-polarized EMW propagates through this photonic structure practically without losses.

Below we analyze numerically both intensity and position of the defect mode inside the first PGB as a function of thickness of SC sublayer for the system under consideration (see

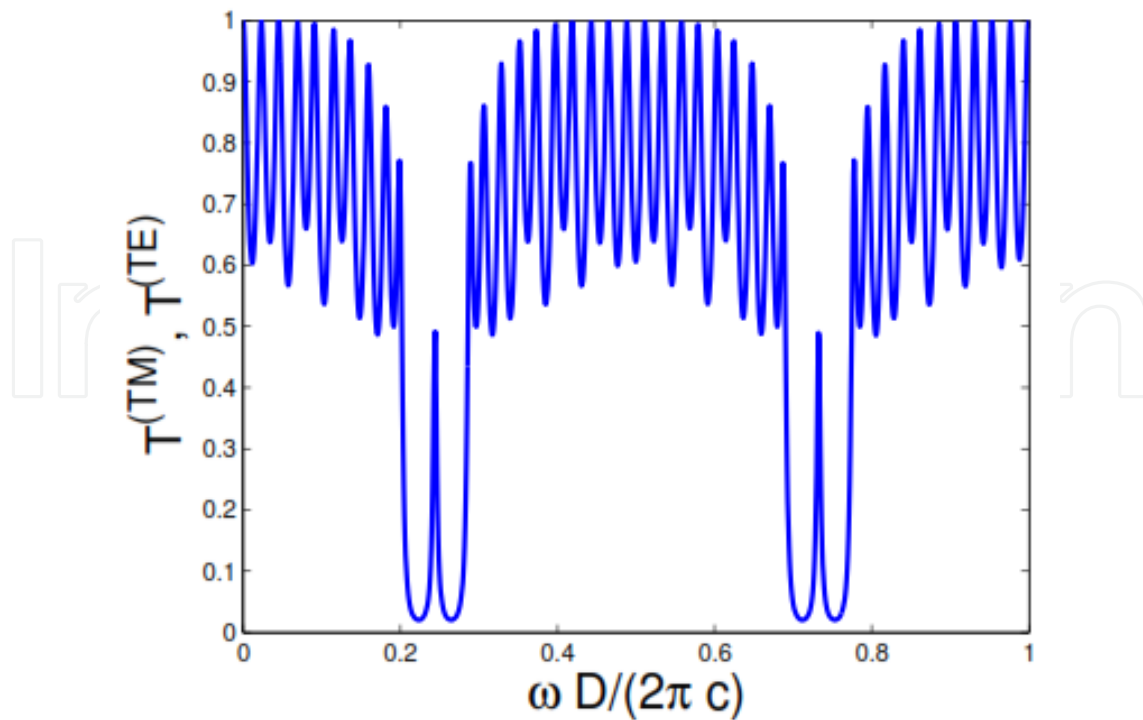


Figure 2. First two PBGs with defect modes located in the centers of forbidden zones. The transmittivities for TE- and TM- modes coincide in the case of defect without SC sublayer.

Fig. 1). From the numerical calculations we obtained, that position and intensity of the defect mode are changing significantly for TM- mode. The corresponding results are presented on Figs. 3 – 6.

We calculated the intensities and positions of both TE- and TM-polarized defect modes inside the first PBG as a function of SC sublayer thickness for different temperatures: $T=4.2\text{ K}$, $T=77\text{ K}$ (below temperature of SC transition) and $T=90\text{ K}$ (at temperature of SC transition). The refractive indices for PC's constituents are equal to $n_1=2.437$, $n_2=1.767$ for $SrTiO_3$ and Al_2O_3 , respectively [28] and the corresponding thicknesses are $d_1=0.42 D$, $d_2=0.58 D$, where PC's period is chosen to be $D=5\text{ }\mu\text{m}$. We varied the SC sublayer thickness in the region between 0 and 70 nm, keeping the thickness of dielectric defect sublayer to be $d_{1d}=0.42 D=2.1\text{ }\mu\text{m}$.

For an estimation of the frequency and temperature dependence of the dielectric tensor of $YBa_2Cu_3O_7$ $\epsilon_{s,v}$ ($v=xx, yy, zz$) (see Eqs. (14) – (16) in paper [18]) we used the following parameters: the scattering rate component $\alpha=1.4\cdot 10^{13}\text{ s}^{-1}$, the London tensor components at absolute zero $\Lambda_{s,x}^{(0)}=2.1\cdot 10^{-30}\text{ s}^2$ and $\Lambda_{s,y}^{(0)}=1.9\cdot 10^{-28}\text{ s}^2$, as well as the half-gap energy at absolute zero $\Delta_0=3.0\cdot 10^{-2}\text{ eV}$ [19].

The results of our calculations for TE-mode are presented in Figs. 3 – 5 and for TM-mode are given in Fig. 6. One can see that the position of TM-polarized defect mode strongly depends on the SC sublayer thickness: the peak of the defect mode shifts to the right edge of the PBG with the increase of d_s .

From Fig. 3 one can see, that at the temperature $T=4.2$ K the defect mode intensity is monotonically increasing with growth of SC sublayer thickness, and the corresponding defect peak approaches the right edge of the PBG.

At higher temperatures ($T=77$ K and $T=90$ K) the intensity of the defect mode first is going down to with growth of d_s and then goes up and merge with the right PBG edge.

In contrast of TM-mode, the defect mode of TE-polarization almost does not change its position under growth of temperature and SC sublayer thickness.

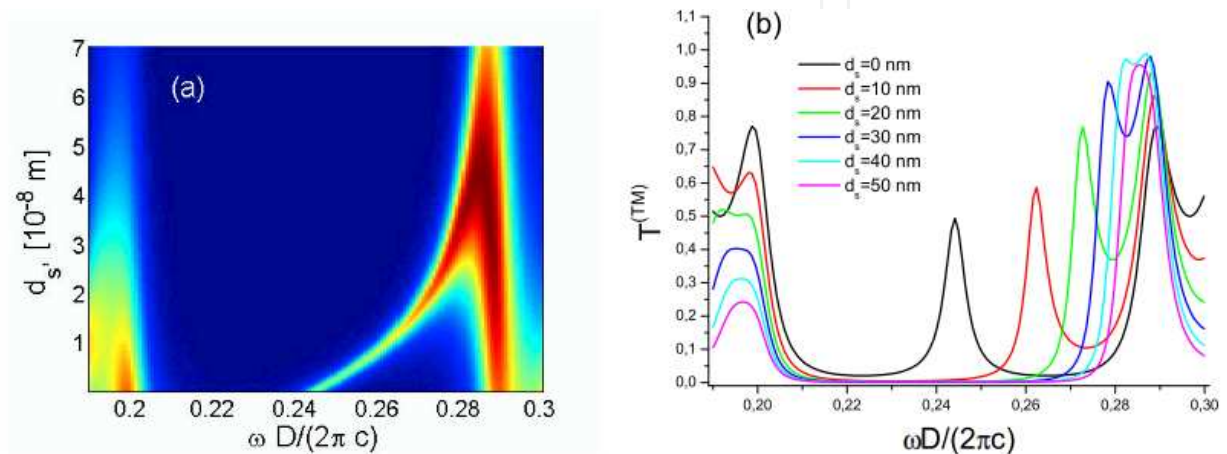


Figure 3. The intensity and position of the TM-polarized defect mode inside the first PBG as function of SC sublayer thicknesses d_s and normalized frequency $\tilde{\omega} = \omega D / (2\pi c)$ at the temperature $T=4.2$ K: (a) the top view; (b): the profiles of the defect mode for different SC sublayer thicknesses.

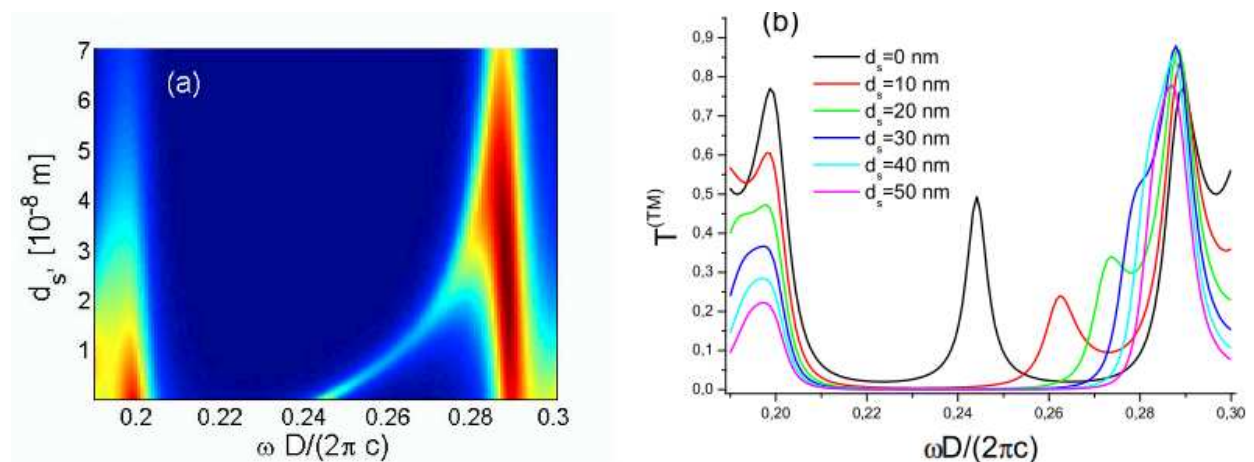


Figure 4. The intensity and position of the TM-polarized defect mode inside the first PBG as function of SC sublayer thicknesses d_s and normalized frequency $\tilde{\omega} = \omega D / (2\pi c)$ at the temperature $T=77$ K: (a) the top view; (b): the profiles of the defect mode for different SC sublayer thicknesses.

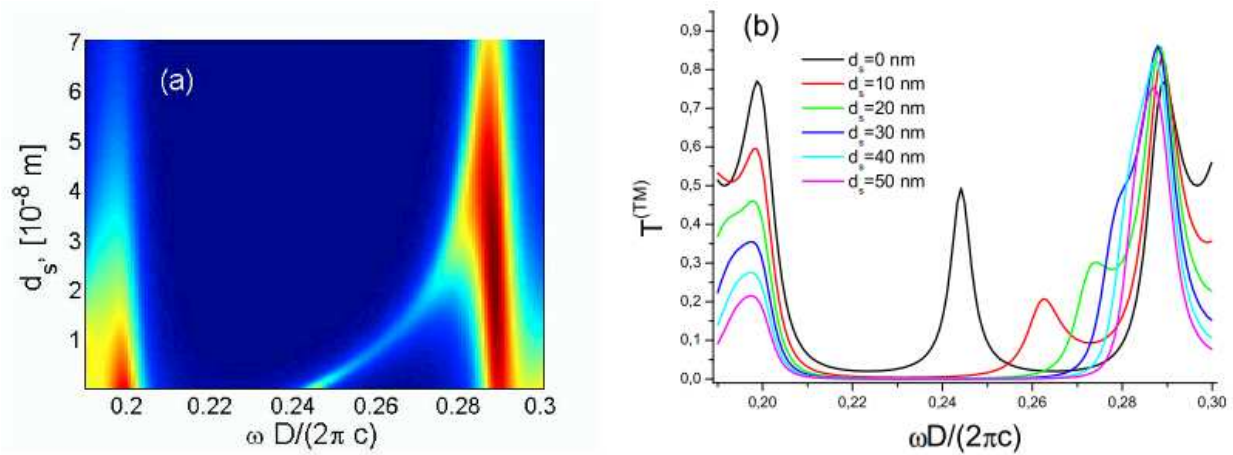


Figure 5. The intensity and position of the TM-polarized defect mode inside the first PBG as function of SC sublayer thicknesses d_s' and normalized frequency $\tilde{\omega} = \omega D / (2\pi c)$ at the temperature $T=90$ K: (a) the top view; (b): the profiles of the defect mode for different SC sublayer thicknesses.

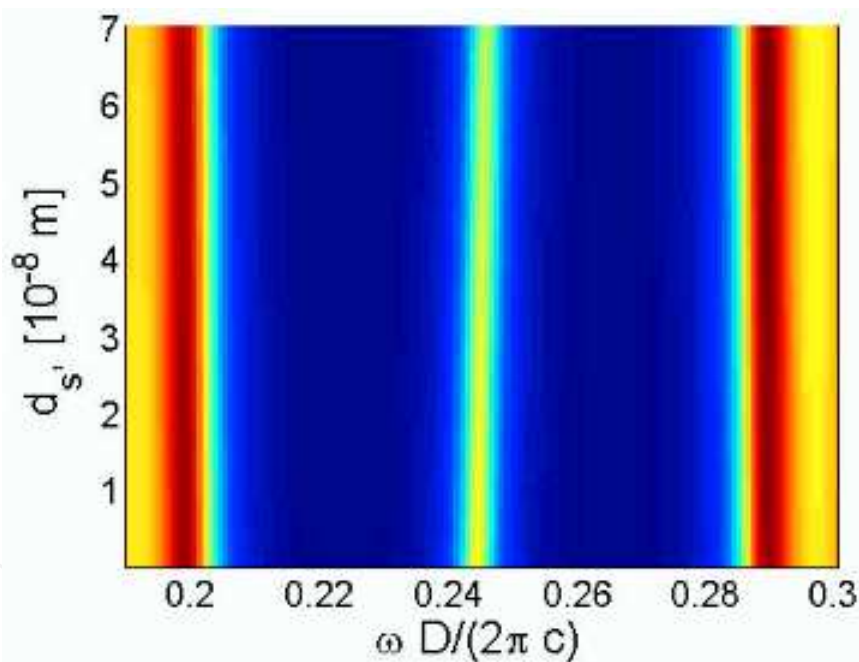


Figure 6. The top view of intensity and position of the TE-polarized defect mode inside the first PBG as function of SC sublayer thicknesses d_s' and normalized frequency $\tilde{\omega} = \omega D / (2\pi c)$.

3. Photonic crystal with two defects

Let us consider a finite size 1D PC of the structure $(BA)^N Def_2(BA)^M Def_1(BA)^N$ consisting of $2N + M$ regular unit cells (BA) with two combined defect layers Def_1 and Def_2 embedded into the PC symmetrically with respect to the PC's edges, as shown in Fig. 1(a). The unit cell with period

$D=d_1+d_2$ of the PC is formed by two dielectric layers: the layer A of strontium titanate $SrTiO_3$ with thickness d_1 , and the layer B of aluminum oxide Al_2O_3 with thickness d_2 . All the layers are located in the xy -plane and the z -axis is perpendicular to the interfaces. Both complex defects Def_1 and Def_2 consist of a $SrTiO_3$ sublayer A_{def} of thickness d_{1d} and a SC defect sublayer $YBa_2Cu_3O_7$ of thickness d_s . The selection of these dielectrics is due to the fact that both $SrTiO_3$ and Al_2O_3 are widely used as substrates for $YBa_2Cu_3O_7$. The medium surrounding the PC is vacuum.

We distinguish the two types of the complex defect layers, depending on the positions of the SC sublayers with respect to the dielectric defect ones: the right-handed (RH) defects $Def_R=A_{def}SC$ and left-handed (LH) defects $Def_L=SC A_{def}$. In Figs. 7(a) – 7(d) we depicted the schematic of four possible geometries of the PCs with two combined SC defects of RH and LH types. The Figs. 7(a) and 7(b) demonstrate the PCs with two RH and two LH defects, which further will be referred to as RH – RH and LH – LH geometries, respectively. The PCs with the SC defects of different types: RH – LH and LH – RH are shown in Figs. 7(c) and 7(d), respectively.

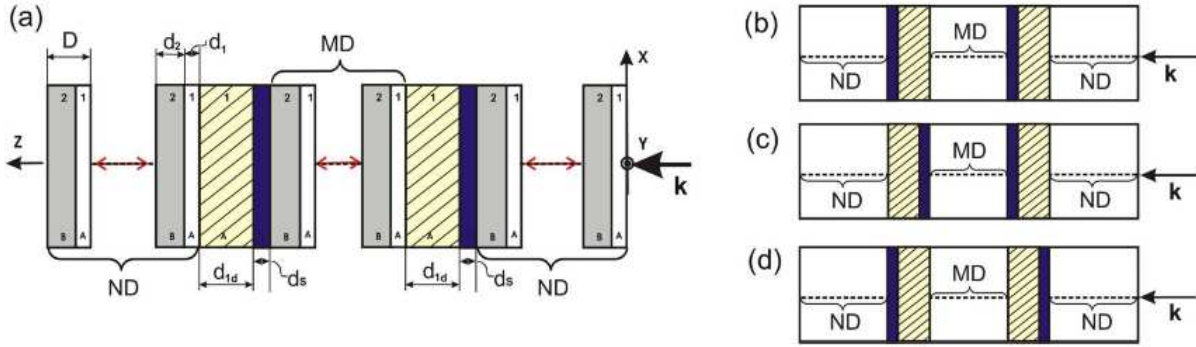


Figure 7. Schematic of finite two-component 1D PCs with two combined SC defect layers: RH – RH (a), LH – LH (b), RH – LH (c), and LH – RH (d) geometries.

Below we present the numerical calculations of the transmittivity spectra of the PCs under consideration as function of the SC defect sublayer thickness d_s , as well as of the dielectric defect sublayer thickness d_1 . Also, we numerically investigate the temperature dependence of the corresponding spectra. We restrict our considerations to the frequency range within the first PBG and its vicinity. For the numerical calculations presented below we chose the same parameters of the PC with unit cell numbers of $N=5$ and $M=2$, as in Sec. 2.

3.1. PC with two RH defects

First, we start our investigation with a PC containing two RH defects (see Fig. 7(a)). In Figs. 8(a) and 8(b) we present the top view of the transmittivities $T^{(x)}$ for the x -polarized EMWs vs the normalized frequency $\tilde{\omega}$ (within the range of the first PBG and its vicinity) and the defect SC sublayer thickness d_s for the liquid helium and liquid nitrogen temperatures: $T=4.2$ K and $T=77$ K, respectively. The SC sublayer thickness d_s varies within the range (0÷70) nm, while the dielectric defect layer thickness is fixed to be $d_{1d}=d_1=2.1$ μ m. The presence of two combined defect layers in the PC leads to the appearance of two narrow DMs inside the PBG (see Figs.

8(a), 8(b)) which are referred to as low-frequency (LF) and high-frequency (HF) DMs. In Fig. 8(c) we plotted the transmittivity spectra for the cases of different SC sublayer thicknesses: $d_s=0, 10, 20, 30, 40$ and 50 nm, calculated for the temperature $T=4.2$ K.

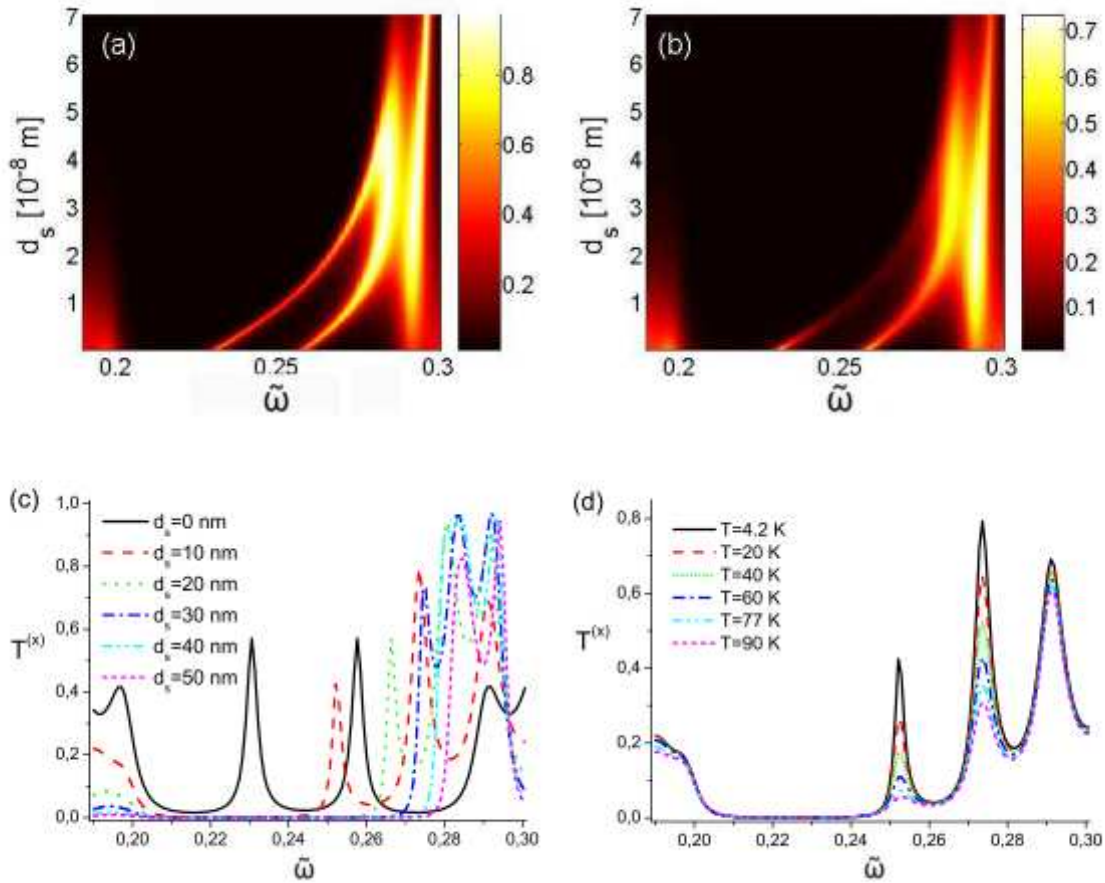


Figure 8. Two RH SC defects. Top view of the transmittivity $T^{(x)}$ vs normalized frequency $\tilde{\omega}$ and the defect SC sublayer thickness d_s for $T=4.2$ K (a) and $T=77$ K (b); the transmittivity spectra for different values of d_s calculated for $T=4.2$ K (c); and the temperature evolution of the transmittivity spectrum for $d_s=10$ nm (d). The results are obtained for the case of the dielectric defect layer with $d_{1d}=d_1=2.1$ μm .

We calculated the frequencies of the PBG edges for the PC with pure dielectric defects (when $d_s=0$): the LF PBG edge is $\tilde{\omega}_{LF}^{PBG}=0.19637$ (which is equivalent to $\omega_{LF}^{PBG}=73.98$ THz or $\lambda_{LF}^{PBG}=25.46$ μm and the HF PBG edge is $\tilde{\omega}_{HF}^{PBG}=0.29107$ (which is equivalent to $\omega_{HF}^{PBG}=109.65$ THz or $\lambda_{HF}^{PBG}=17.18$ μm). According to this estimation the first PBG's width is $\Delta\omega_{PBG}=35.68$ THz, which corresponds to $\Delta\lambda_{PBG}=8.28$ μm . In the case of pure dielectric defects ($d_s=0$ nm) the DMs are localized inside the PBG symmetrically with respect to the PBG edges at the normalized frequencies $\tilde{\omega}_{LF}^{peak}=0.23059$ (which is equivalent to $\omega_{LF}^{peak}=86.87$ THz or $\lambda_{LF}^{peak}=21.68$ μm) and $\tilde{\omega}_{HF}^{peak}=0.25765$ ($\omega_{HF}^{peak}=97.06$ THz or $\lambda_{HF}^{peak}=19.41$ μm) and their magnitudes practically coincide: $T_{LF}^{(x)} \approx T_{HF}^{(x)} \approx 0.57$ as shown by the black solid line in Fig. 8(c). The presence of the SC sublayer

breaks the symmetry of the position and values of the DM's peaks. The increase of d_s leads to an essential shift of the DMs to the HF PBG edge up to their mergence near the HF PBG edge for $d_s \approx 40$ nm, as one can see in Figs. 2(a), 2(b) and 2(c). For example, for $d_s=10$ nm, the LF and HF peaks positions become $\tilde{\omega}_{LF}^{peak} = 0.25207$ (which is equivalent to $\omega_{LF}^{peak} = 94.96$ THz or $\lambda_{LF}^{peak} = 19.83$ μm) and $\tilde{\omega}_{HF}^{peak} = 0.25765$ ($\omega_{HF}^{peak} = 103.06$ THz or $\lambda_{HF}^{peak} = 18.28$ μm), respectively. The frequency shifts of the LF and HF DMs are $\Delta\tilde{\omega}_{LF} = 0.02148$ (which is equivalent to $\Delta\omega_{LF}^{peak} = 8.09$ THz or $\Delta\lambda_{LF}^{peak} = 2.27$ μm) and $\Delta\tilde{\omega}_{HF} = 0.01591$ ($\Delta\omega_{HF}^{peak} = 6.02$ THz or $\Delta\lambda_{HF}^{peak} = 1.55$ μm) which are about 27.4% and 18.7% of the PBG width at $d_s=0$ nm, respectively. The distance between the DMs decreases considerably with the increase of the SC sublayer thickness: from $\Delta\tilde{\omega} = 0.02706$ ($\Delta\omega^{peak} = 10.19$ THz or $\Delta\lambda^{peak} = 2.27$ μm) for $d_s=0$ to $\Delta\tilde{\omega} = 0.02149$ ($\Delta\omega^{peak} = 8.01$ THz or $\Delta\lambda^{peak} = 1.55$ μm) for $d_s=10$ nm and to $\Delta\tilde{\omega} = 0.01432$ ($\Delta\omega^{peak} = 5.39$ THz or $\Delta\lambda^{peak} = 0.96$ μm) for $d_s=20$ nm, to $\Delta\tilde{\omega} = 8 \cdot 10^{-3}$ ($\Delta\omega^{peak} = 2.99$ THz or $\Delta\lambda^{peak} = 0.51$ μm) for $d_s=30$ nm.

The SC sublayer thickness increase also leads to an abrupt reduction of the transmittivity value at the LF PBG edge. The HF PBG edge position changes as well, slightly moving to higher frequencies with increasing of d_s and reaching the maximum value $T^{(x)} \approx 0.96$ for $d_s=40$ nm. From Fig. 8(a) one can see that for the SC defect layer thickness $d_s=40$ nm both DMs merge. The amplitudes of the peaks vary as well: the transmittivity at the HF DM grows with the increase of d_s , while the LF peak intensity first goes down to $T_{\min}^{(x)} \approx 0.42$ (at $\tilde{\omega} \approx 0.252$) for $d_s=10$ nm, while after that, its amplitude also increases with further increase of d_s .

The DMs intensities change considerably with increasing temperature. Comparing Figs. 8(a) and 8(b), one can see that the influence of temperature on the PBG spectra is especially pronounced near the DM frequencies. In Fig. 8(d) the evolution of the transmittivity spectrum of the x -polarized EMW is given. We calculated the transmittivity profiles for the PC with the SC sublayer of fixed thickness $d_s=10$ nm, at temperatures $T=4.2$ K, $T=20$ K, $T=40$ K, $T=60$ K, $T=77$ K, and $T=90$ K. As follows from Fig. 8(d), the transmittivities of both LF and HF DMs drop down with increasing temperature, but the LF peak becomes visibly weaker than the HF one for temperatures above $T=77$ K. Meanwhile, the temperature practically does not affect the DM positions. At $T=4.2$ K the transmittivities of the LF and HF DMs are $T_{LF}^{(x)} \approx 0.42$ and $T_{HF}^{(x)} \approx 0.79$. At $T=20$ K they become $T_{LF}^{(x)} \approx 0.27$ and $T_{HF}^{(x)} \approx 0.65$, respectively. At $T=77$ K the LF peak drops to a vanishingly small value of $T_{LF}^{(x)} \approx 0.07$, and further it practically flattens at $T=90$ K, while the HF one still stays relatively large: $T_{HF}^{(x)} \approx 0.35$. One can see that the change of temperature produces only a slight effect on both PBG edges.

In Fig. 9(a) and 9(b) we present the transmittivity spectrum dependence on d_s for y -polarized DM, calculated for $T=4.2$ K (the top-view and profiles, respectively).

In contrast to the case of the x -polarized DMs given in Figs. 8(a) and 8(c), the transmittivity of the y -polarized DM practically does not depend on the SC defect sublayer thickness, when d_s is about several tens of nanometers.

The transmittivity spectra of the PCs are also sensitive to the thickness of the dielectric defect sublayer d_{1d} . In Figs. 9(a) and 9(b) the top-views of $T^{(x)}$ as function of the normalized thickness

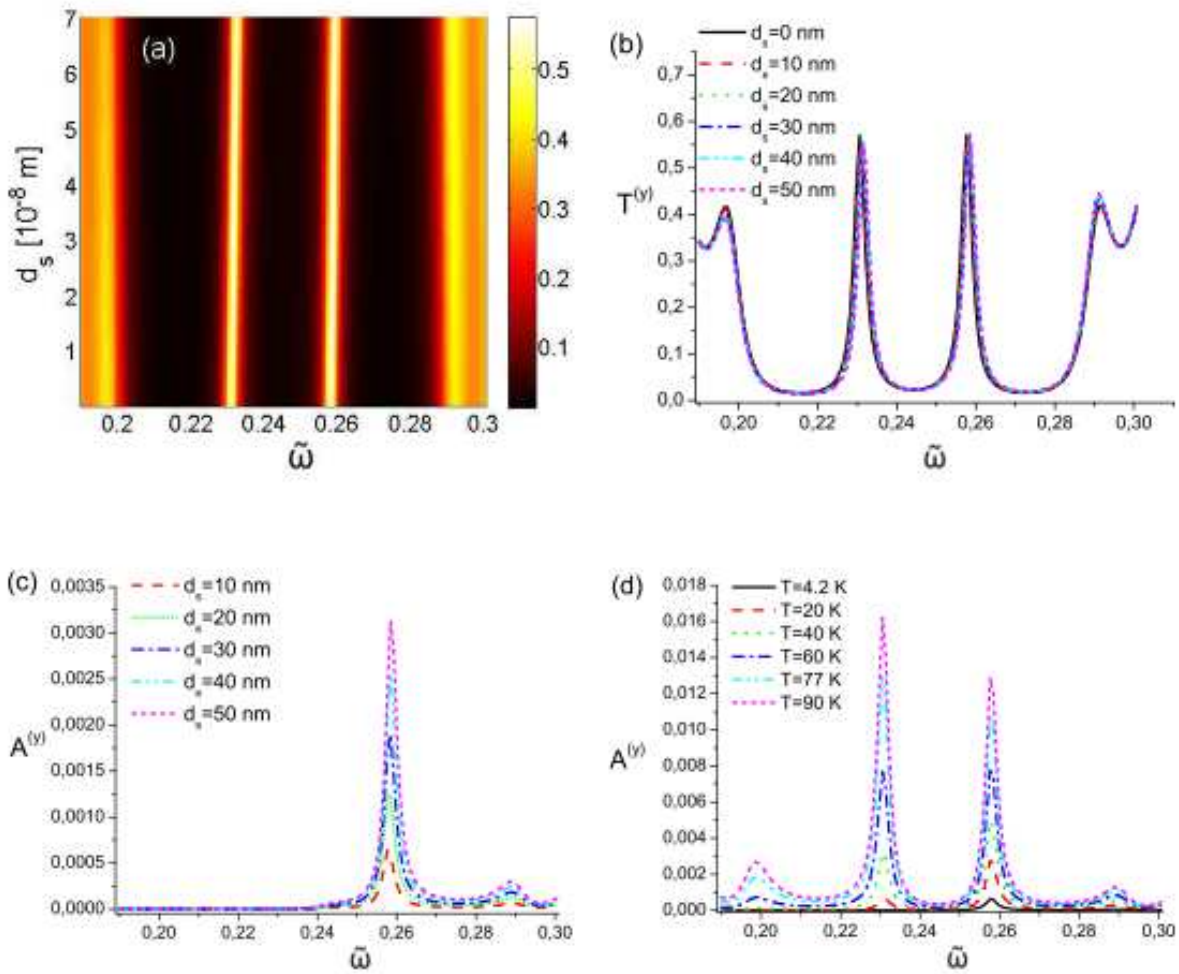


Figure 9. Two RH SC defects. Top view of the transmittivity $T^{(y)}$ vs normalized frequency $\tilde{\omega}$ and defect SC sublayer thickness d_s for $T=4.2$ K (a); transmittivity $T^{(y)}$ (b) profiles for different d_s calculated for $T=4.2$ K. The results are obtained for the case of the dielectric defect layer with $d_{1d}=d_{1r}=2.1$ μm .

of the dielectric sublayer d_{1d}/D and normalized frequency $\tilde{\omega}$ are presented for the PCs with the SC defect sublayers thicknesses $d_s=10$ nm and $d_s=20$ nm. From Figs. 9(a) and 9(b) one can see that the thickness increase of both dielectric defect sublayers results in a shift of the DMs to the LF PBG edge. It should be mentioned, that the analogous increase of the SC defect sublayers d_s leads to a shift of the DMs in the opposite direction, i.e. to the HF PBG edge. This shift becomes noticeable in the scale of a few tens of percents of the period D .

The other peculiarity of the dependence of $T^{(x)}$ on d_{1d} is its periodicity. Comparing Figs. 10(a) and 10(b), one can see that the increase of d_s leads to a narrowing of the DMs and to their decaying (the HF DM decays stronger).

Above we investigated the PC with two identical complex (SC + dielectric) defects but with different thicknesses of SC sublayers. We can fix one of the SC sublayer thickness d_{sR} or d_{sL} (in the left or right combined defect, respectively) and vary the other SC sublayer thickness to obtain a possible changing of the PBG spectra. In Figs. 11(a) – 11(c) we present top views of

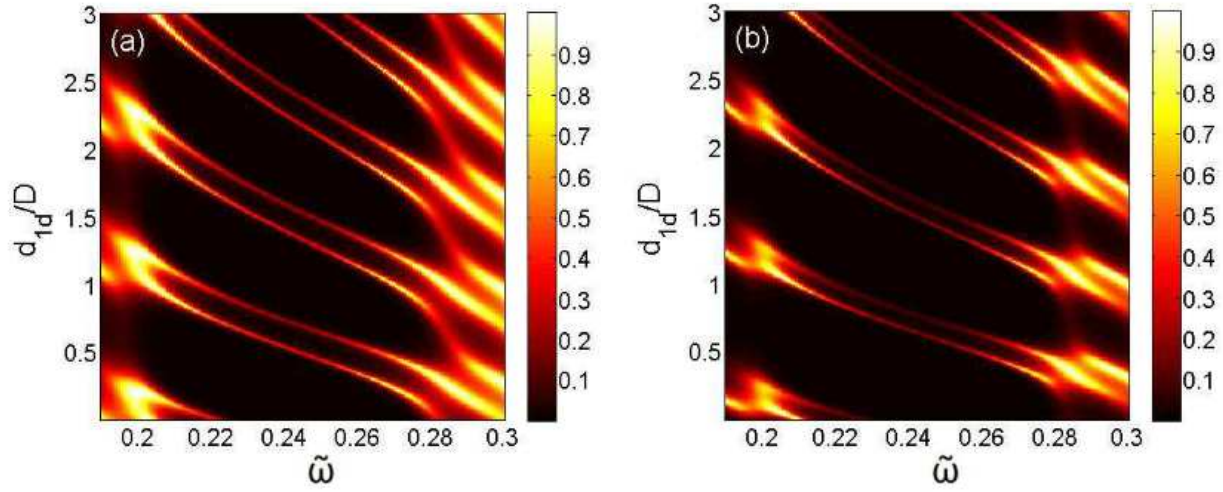


Figure 10. Two RH SC defects. Top view of the transmittivity T^x vs normalized frequency $\tilde{\omega}$ and normalized thickness d_{1d}/D for $d_s=10$ nm (a); and $d_s=20$ nm (b). The calculations are performed for $T=4.2$ K.

the transmittivity of x -polarized EMWs T^x as function of $\tilde{\omega}$ and d_{sR} when the left-side SC defect thickness is fixed to $d_{sL}=10$ nm (a), $d_{sL}=20$ nm (b), and $d_{sL}=30$ nm (c).

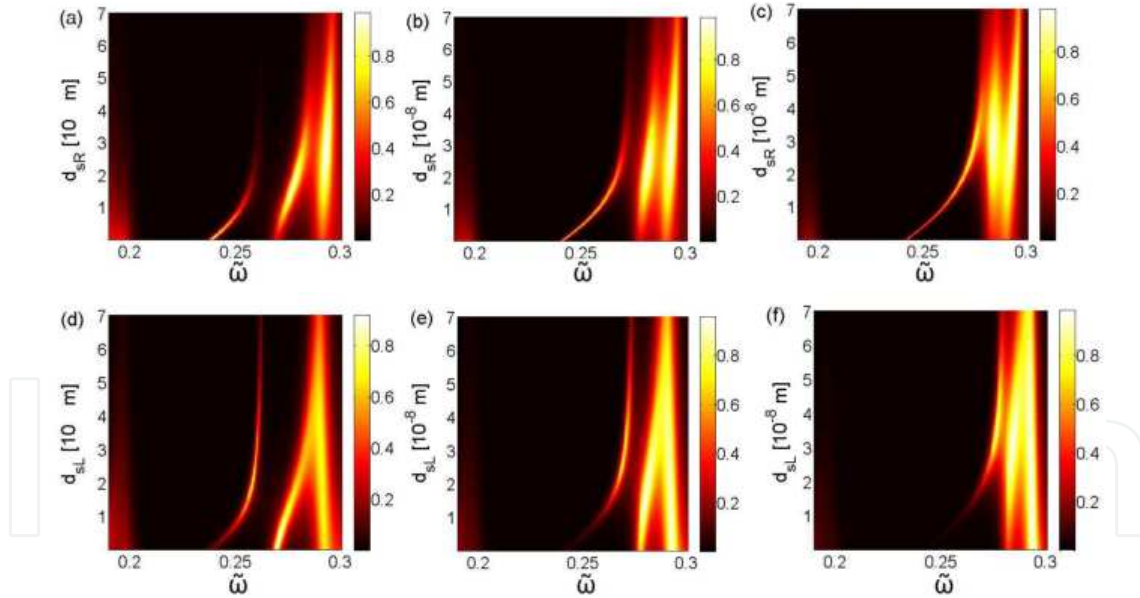


Figure 11. Two RH SC defects. Top view of transmittivity T^x vs normalized frequency $\tilde{\omega}$ and thickness of the RH or LH SC defect sublayers (d_{sR} or d_{sL} , respectively). For the case of fixed LH SC defect layers with (a) $d_{sL}=10$ nm, (b) $d_{sL}=20$ nm, and (c) $d_{sL}=30$ nm; and for the case of fixed RH SC defect layers with (d) $d_{sR}=10$ nm, (e) $d_{sR}=20$ nm, and (f) $d_{sR}=30$ nm. The calculations are performed for $T=4.2$ K, $d_{1d}=d_1$, and $N=5$, $M=2$.

The corresponding spectra for the opposite case (with fixed thickness of the right-side SC defect $d_{sR}=10$ nm, 20 nm, and 30 nm) are given in panels (d), (e), and (f), respectively. Comparing Figs. 8(a) and 11(a) for symmetrical and asymmetrical changes of the SC defect layers thickness,

one can see that the behavior of the DMs changed. In contrast to the case of identical SC sublayers given in Figs. 8(a), for the case of fixed $d_{sL}=10$ nm the LF DM is more narrow and it decays fast with increasing of d_{sL} , not merging with the HF PBG edge as shown in Fig. 8(a). With the increase of the fixed value of d_{sL} to 20 nm (Fig. 11(b)) the HF DM comes closer to the HF PBG edge and merges with it for $d_{sL}=30$ nm for all values of d_{sR} . For $d_{sL}=20$ nm and $d_{sL}=30$ nm the LF DM grows with increasing of d_{sR} (Figs. 11(b) and 11(d)) and merges with the HF PBG edge for $d_{sL}=30$ nm at about $d_{sR}=40$ nm. Varying the left-side SC defect layer thickness one can obtain another dependence of the spectra on d_{sL} (Figs. 11(d) – 11(f)). For this situation the LF DM becomes visible for larger values of d_{sL} . The tendency of the shift of DM to higher frequencies with the increase of both d_{sL} and d_{sR} remains.

3.2. PC with two LH defects

In this subsection we present the numerical results for the PC with two LH defect layers depicted schematically in Fig. 7(b). Similar to the previous case, we study the EMW's incidence on the right-hand surface of the PC, and all the parameters of the PC are the same, as described in detail above in section 3.1, except for the replacing of the RH combined defects to LH ones.

In Figs. 12(a) – 12(d) we present the resulting transmittivities $T^{(x)}$ for the PC with two LH defects, analogous to that of Figs. 8(a) – 8(d).

In Figs. 12(a) and 12(b) one can see the top view of the transmittivities vs the normalized frequency and the defect SC sublayer thickness d_s for the temperatures $T=4.2$ K and $T=77$ K, respectively. The SC sublayer thickness d_s varies in the range (0 ÷ 70) nm, while the dielectric defect layer thickness is fixed to be $d_{1d}=d_1=2.1$ μm . In Fig. 12(c) we demonstrate the evolution of the transmittivity profiles $T^{(x)}$ with the increase of d_s .

Comparing the corresponding parts of Figs. 12 and 8, one can see that the behavior of the transmittivity $T^{(x)}$ has drastically changed. Though analogously to the case of the PC with two RH defects, both DMs have a tendency to shift to higher frequencies with the increase of d_s , now this shift is substantially smaller. The solid lines in Fig. 12(c) and 8(c) denote the transmittivity spectrum for $d_s=0$ nm and are equivalent. For $d_s=10$ nm the LF and HF peak positions become $\tilde{\omega}_{LF}^{peak}=0.23218$ (which is equivalent to $\omega_{LF}^{peak}=87.47$ THz or $\lambda_{LF}^{peak}=21.53$ μm) and $\tilde{\omega}_{HF}^{peak}=0.2524$ ($\omega_{HF}^{peak}=97.66$ THz or $\lambda_{HF}^{peak}=19.28$ μm), respectively. The frequency shifts of the LF and HF DMs are practically the same $\Delta\tilde{\omega}_{LF}\approx\Delta\tilde{\omega}_{HF}=0.0016$ (which is equivalent to $\Delta\tilde{\omega}_{LF}^{peak}=0,6$ THz or $\Delta\lambda_{LF}^{peak}=0.15$ μm) which is about 1.8% of the PBG width at $d_s=0$ nm. In contrast to the case of the 1D PC with two RH defects, the distance between the DMs practically does not change with the increase of the SC sublayer thickness remaining about $\Delta\tilde{\omega}^{peak}\approx 0.0271$ ($\Delta\omega^{peak}\approx 10.21$ THz or $\lambda^{peak}\approx 2.25$ μm) for d_s varying within the range of (0 ÷ 70) nm. Moreover, in this geometry the DMs do not merge with the HF PBG edge when d_s varies within some tens of nanometers, as was obtained in the case with double RH defects. In addition, the LF PBG edge splits when d_s exceeds the value of about 10 nm and then one branch significantly approaches the LF DM with increasing of d_s and merges with it at $d_s\approx 40$ nm. The intensity of the LF DM increases with the increase of d_s , from $T=0.6$ for the case of purely dielectric defect layers ($d_s=0$

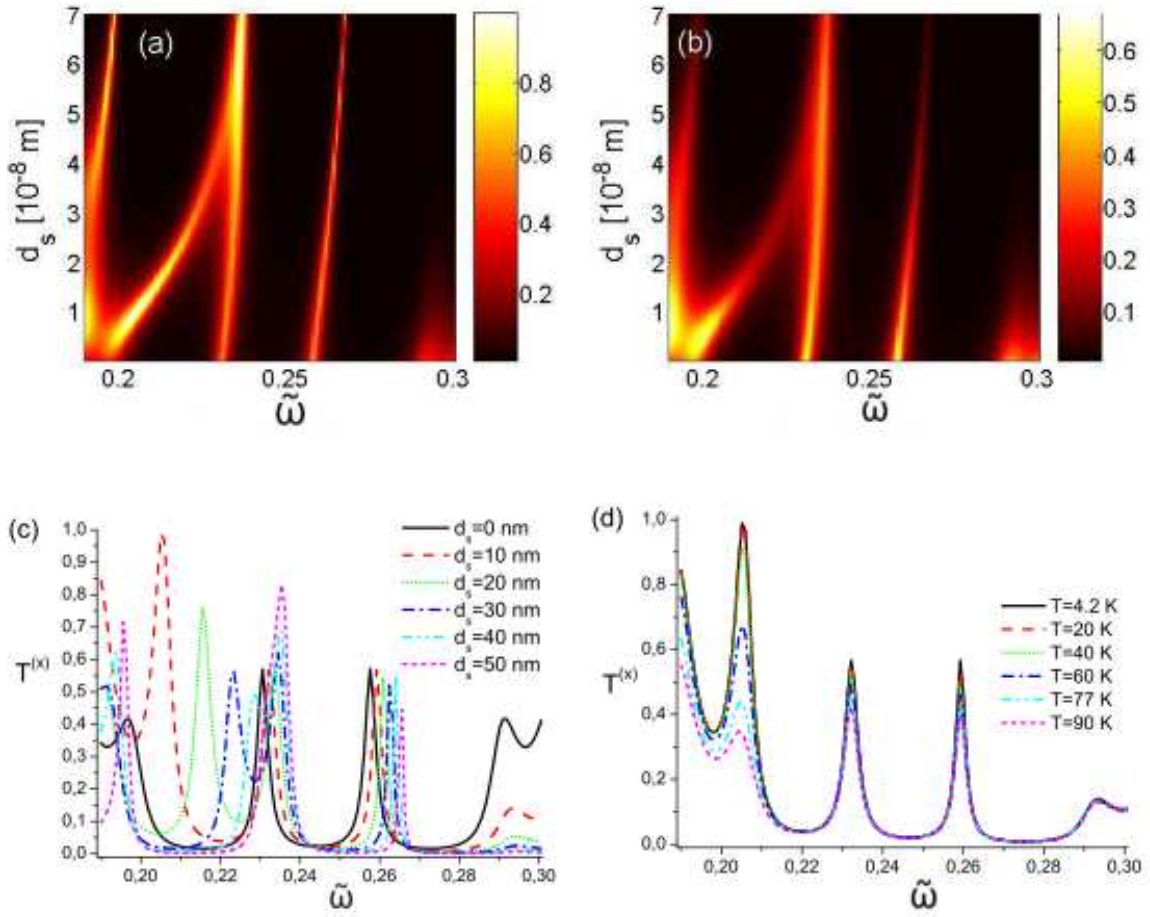


Figure 12. Two LH SC defects. The same as in Fig. 8, except for the case of LH SC defects.

nm) to $T=0.85$ for $d_s=50$ nm. The HF PBG edge decays fast with the increase of d_s , in contrast to the case of RH defects, where the maximum values of $T^{(x)}$ are achieved at the HF PBG edge.

In Fig. 12(d) one can see the evolution of the transmittivity spectra of the first PBG with changing temperature. The results are given for the PC with the SC defect sublayers and the dielectric defect ones $d_s=10$ nm and $d_{1d}=2.1$ μm , respectively. As follows from Fig. 12(d), the maximum influence of the temperature on the $T^{(x)}$ spectrum takes place at the LF PBG edge, where the transmittivity drops from $T_{LF, PBG}^{(x)}=0.99$ at $T=4.2$ K to $T_{LF, PBG}^{(x)}=0.34$ at $T=90$ K. The behavior of the DM's peaks with temperature increase is similar, but much less pronounced: the transmittivity slightly diminishes from $T_{LF}^{(x)} \approx 0.57$ at $T=4.2$ K to $T_{LF}^{(x)}=0.42$ and $T_{HF}^{(x)}=0.40$. The HF PBG edge practically does not experience any affect of the temperature variation within the interval from 4.2 K to 90 K.

As for the behavior of the transmittivity of the y -polarized light $T^{(y)}$, it practically does not depend on the type of defects (RH or LH) in the PC, and its variation with increasing temperature and d_s remains similar as depicted in Fig. 9(a) for the PC with two RH defects.

Examining the transmittivity spectra dependence on the normalized thickness of the dielectric sublayer d_{1d}/D , analogously to the case investigated above for the 1D PC with two RH defects, we obtained the periodically repeating structures in the top views of $T^{(x)}$ vs $\tilde{\omega}$ and d_{1d} (Figs. 13(a) and 13(b)). As before, the spectra variations with d_{1d} are calculated for the SC defect sublayer fixed to be $d_s=10$ nm (Fig. 13(a)) and $d_s=20$ nm (Fig. 13(b)). The thickness increase of both dielectric defect sublayers results in a shift of the DMs to the LF PBG edge, as it was obtained above for a 1D PC with two RH defects. But for a 1D PC with two LH defects, one can see the distortion of the DMs on the LF PBG edge with the increase of d_s to 20 nm. A further enlargement of d_s leads to the DM's lines breaking.

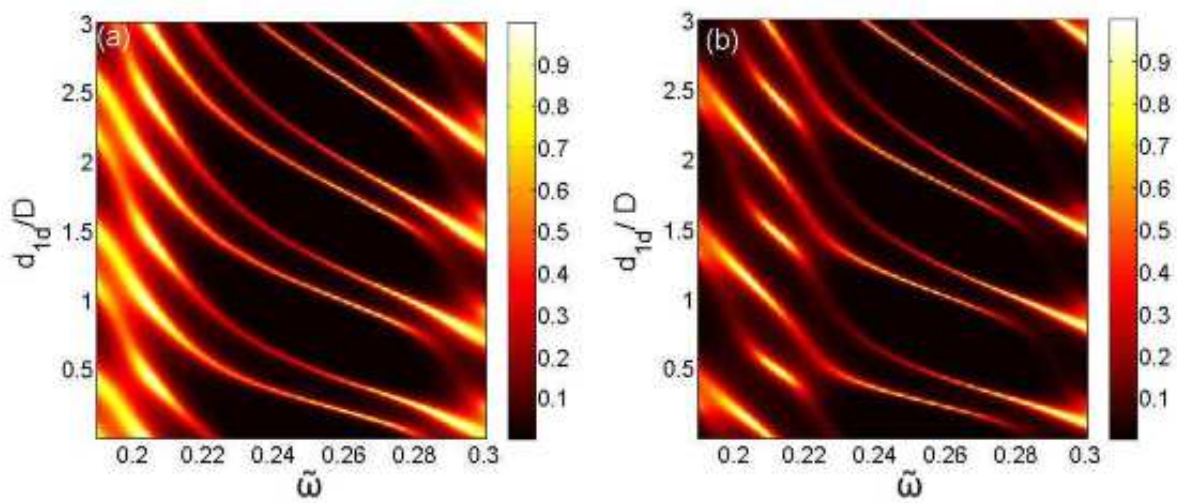


Figure 13. The same as for Fig. 11, except for the case of two LH SC defects.

In Figs. 14(a) – 14(c) we show the top views of transmittivity $T^{(x)}$ versus $\tilde{\omega}$ (within the 1st PBG) and SC defect layer thicknesses d_{sR} (left SC defect sublayer). Varying d_{sR} from 0 to 70 nm we keep the thickness of the left-sided SC defect sublayer fixed to be (a) $d_{sL}=10$ nm, (b) $d_{sL}=20$ nm, and (c) $d_{sL}=30$ nm. The calculations of $T^{(x)}$, presented in Figs. 14(d) – 14(f), are performed for $T=4.2$ K and dielectric defect sublayers of thickness $d_{1d}=d_1=2.1$ μm for a PC structure with the period numbers $N=5$ and $M=2$. Comparing Figs. 14(a) – 14(c) with Fig. 12(a), we see that in the case of asymmetrical SC defects the LF PBG edge does not merge with the LF DM when we change the right-sided SC defect sublayer thickness d_{sR} . Varying d_{sL} while d_{sR} is fixed we obtain a merge of the decreasing LF DM with the LF PBG edge for $d_{sR}=30$ nm, similar to that in Fig. 12(a) for $d_{sL} \approx 60$ nm (Fig. 14(f)).

Considering asymmetrical changes of the SC defect sublayer thicknesses, as it was done analogously for the case of two RH defects in section 3.1, for the case of a 1D PC with two LH we obtain different spectra when changing one of the SC defect thicknesses while the other one is fixed.

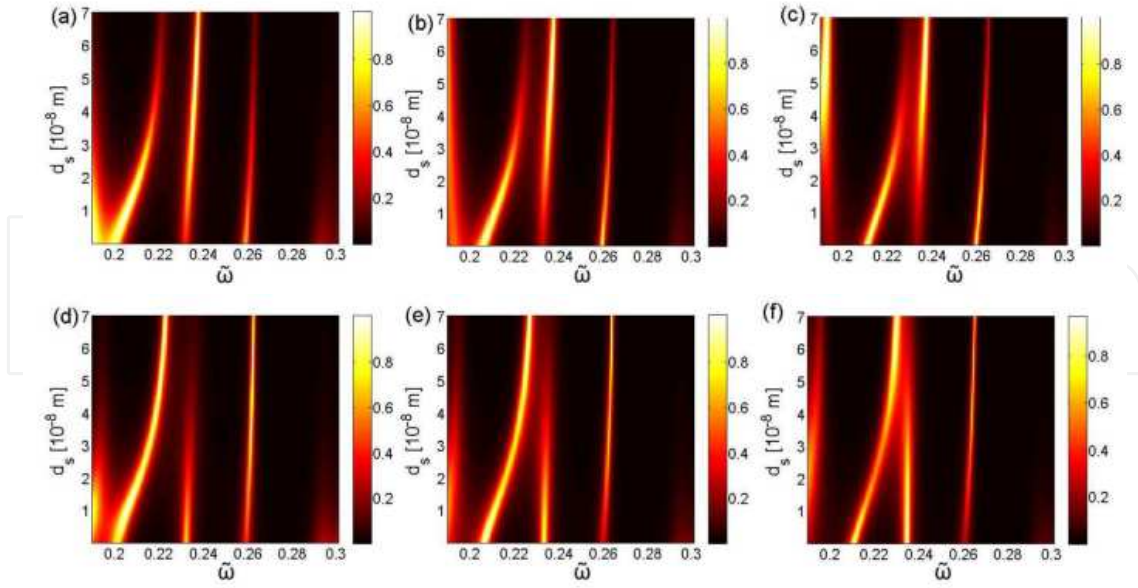


Figure 14. The same as for FIG. 11, except for LH – LH geometry.

3.3. PC with RH – LH and LH – RH defects

In this subsection we present the numerical results for the PCs with two defect layers depicted schematically in Fig. 7(c) and (d). In Figs. 15(a) and 15(b) we present the top view of the transmittivities $T^{(x)}$ for the x -polarized EMWs vs the normalized frequency $\tilde{\omega}$ and the defect SC sublayer thickness d_s for RH – LH and LH – RH geometries, respectively.

The SC sublayer thickness d_s varies within the range $(0 \div 70)$ nm, while the dielectric defect layer thickness is fixed to be $d_{1d}=d_1=2.1$ μm . The color in Figs. 2(a) and 2(b) denotes the value of the transmittivity, as shown on the panels. The results are obtained for temperature $T=4.2$ K. The presence of two combined defect layers in the PC leads to appearance of two narrow DMs inside the PBG (see Figs. 15(a), 15(b)) which further are referred to as low-frequency (LF) and high-frequency (HF) DMs.

As one can see from Figs. 15(a) and 15(b), for both geometries (RH – LH and LH – RH), the increase of d_s from 0 to 70 nm leads to a shift of both LH and HF DMs to higher frequencies, but the shifts of HF DMs are larger than of the LF ones.

In the case of RH – LH geometry, first the LF defect mode slightly deviates to higher frequencies with increasing d_s and further, after $d_s \approx 20$ nm, the LF DM gets thin and its position does not change with further increase of d_s , while the HF DM peak merges with the HF PBG edge and the transmittivity values of both HF PBG edge and HF DM decrease. For all values of d_s from the considered interval (except $d_s=0$ nm) the LF defect mode is more pronounced than the HF one.

For the case of LH – RH geometry, the behavior of the defect modes is opposite: the LF defect mode is less pronounced than the HF one. For $d_s=10$ nm the LF DM is about 8 times smaller in

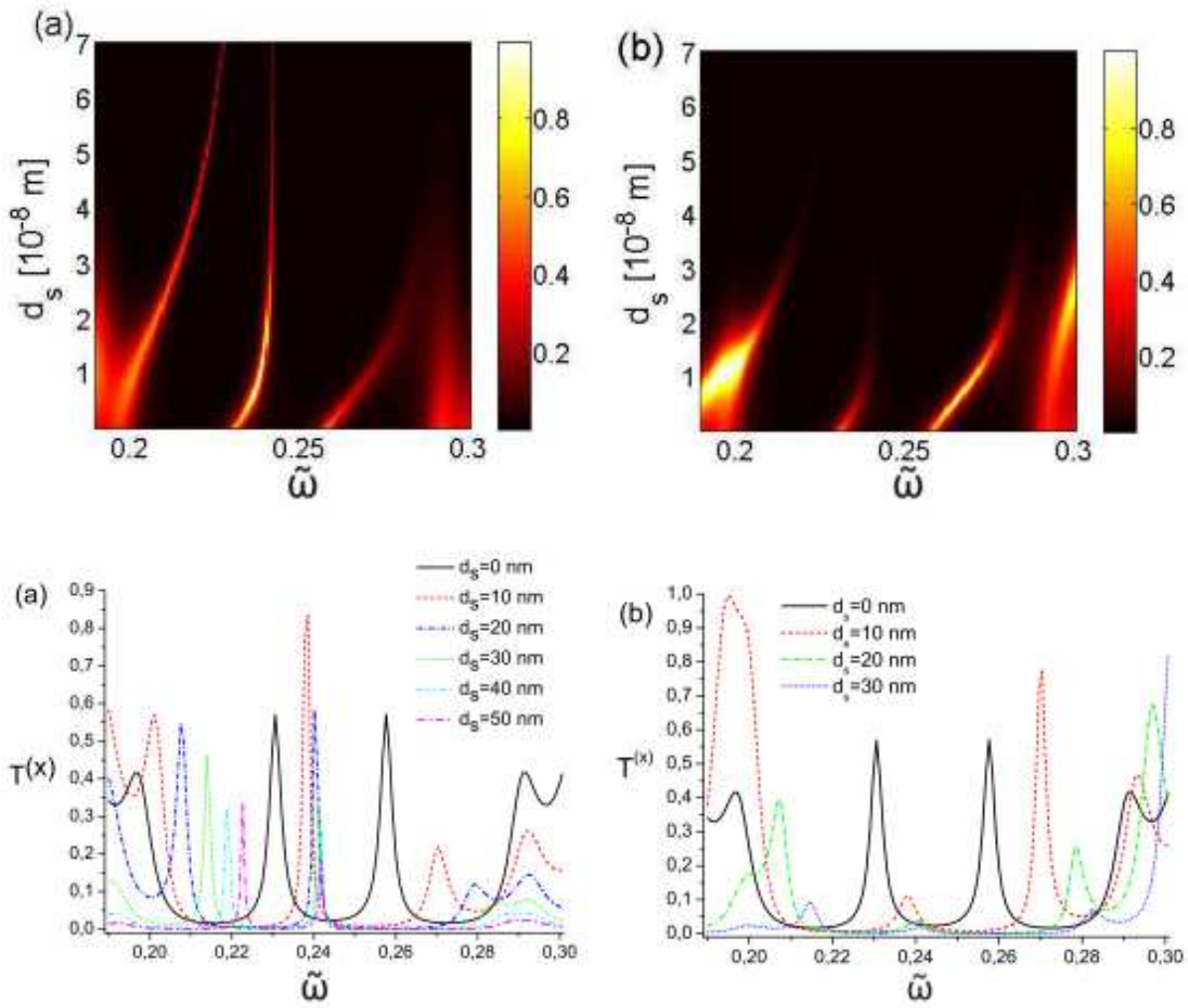


Figure 15. Top view of the transmittivity $T^{(x)}$ vs normalized frequency $\tilde{\omega}$ and the defect SC sublayer thickness d_s for the cases of RH – LH (a) and LH - RH defect layers (b). The transmittivity spectra $T^{(x)}$ for different values of the SC sublayer thicknesses for the RH – LH (a) and LH - RH geometries (b). The results are obtained for the case of the dielectric defect layer $d_{it}=2.1 \mu\text{m}$ and temperature $T=4.2 \text{ K}$.

magnitude then the HF DM, and for $d_s > 20 \text{ nm}$ the LF DM is practically suppressed, while the HF DM still exists up to $d_s = 30 \text{ nm}$.

In Figs. 15(c) we give the transmittivity $T^{(x)}$ spectra for $d_s = 0$ (solid lines), $d_s = 10 \text{ nm}$ (dashed lines), $d_s = 20 \text{ nm}$ (dash-dotted lines), $d_s = 30 \text{ nm}$ (dotted lines), $d_s = 40 \text{ nm}$ (dash-dot-dotted lines), and $d_s = 50 \text{ nm}$ (long dash-dotted lines) for the case of RH – LH geometry. In the case of LH – RH geometry, for d_s increasing 30 nm the both DMs are suppressed and in Fig. 15(d) we show the $T^{(x)}$ spectra only for $d_s = 0$ (solid lines), $d_s = 10 \text{ nm}$ (dashed lines), $d_s = 20 \text{ nm}$ (dash-dotted lines), and $d_s = 30 \text{ nm}$ (dotted lines). Obviously, in the case of pure dielectric defects ($d_s = 0$) the spectra for RH – LH and LH – RH geometries are identical (the solid lines in Figs. 15(c) and 15(d)). In this case two DM peaks of equal values $T_{LF}^{(x)} = T_{HF}^{(x)} \approx 0.57$ are localized symmetrically inside the PBG at $\tilde{\omega}_{LF}^{peak} = 0.2307$ and $\tilde{\omega}_{HF}^{peak} = 0.2577$ which correspond to $\omega_{LF}^{peak} = 86.91 \text{ THz}$ and $\omega_{HF}^{peak} = 97.08$

THz, respectively. For $d_s=0$ the positions of the PBG edges are $\tilde{\omega}_{LF}^{PBG}=0.1967$ ($\omega_{LF}^{PBG}=74.10$ THz) and $\tilde{\omega}_{HF}^{PBG}=0.2915$ ($\omega_{HF}^{PBG}=109.82$ THz), so the PBG width is $\Delta\tilde{\omega}_{PBG}=0.0948$ ($\Delta\omega_{PBG}=35.71$ THz), and the transmittivity values at both PBG edges are equal: $T_{LF}^{(x)PBG}=T_{HF}^{(x)PBG}\approx 0.41$.

The introduction of the SC sublayers into a PC with two dielectric defect layers changes the symmetry of the positions and values of DMs, as well as of the PBG edges. For example, the SC sublayers of thicknesses $d_s=10$ nm drastically change the transmittivity spectra. As one can see from Figs. 15(c) and 15(d), both DM peaks shifts to higher frequencies. For the RH – LH geometry at $d_s=10$ nm the DM peaks are located at $\tilde{\omega}_{LF}^{peak}=0.2385$ ($\omega_{LF}^{peak}=89.85$ THz) and $\tilde{\omega}_{HF}^{peak}=0.2705$ ($\omega_{HF}^{peak}=101.90$ THz). So, the LF DM shift from its position at $d_s=0$ is $\Delta\tilde{\omega}_{LF}^{peak}\approx 0.0078$ ($\Delta\omega_{LF}^{peak}\approx 2.94$ THz), while the HF DM shift is $\Delta\tilde{\omega}_{HF}^{peak}\approx 0.0128$ ($\Delta\omega_{HF}^{peak}\approx 0.48$ THz). The distance between the DM peaks becomes $\Delta\omega^{peak}\approx 0.0317$ (approximately 11.94 THz), which is by 17% larger than for the case of pure dielectric defect layers.

For the RH – LH geometry increasing d_s leads to a shrinking of the PBG width: the LH PBG edge shifts to higher frequencies, while the HF PBG edge remains at its position. So, the PBG width for d_s to 10 nm is $\Delta\tilde{\omega}_{PBG}\approx 0.08063$, which is about 30.38 THz which is 15% of the PBG width at $d_s=0$. One can be mentioned that for both RH – LH and LH – RH geometries the PBG spectra variation with increasing d_s is quite different from the cases described in the previous subsection, where we considered the asymmetrical configurations RH – RH and LH – LH.

In Figs. 16(a) and 16(b) we show the transmittivity $T^{(x)}$ evolution with changing temperature for the PCs of RH – LH and LH – RH geometries, respectively. The spectra are calculated for the defect sublayer thicknesses $d_s=10$ nm and $d_{1d}=d_{1l}=2.1$ μm .

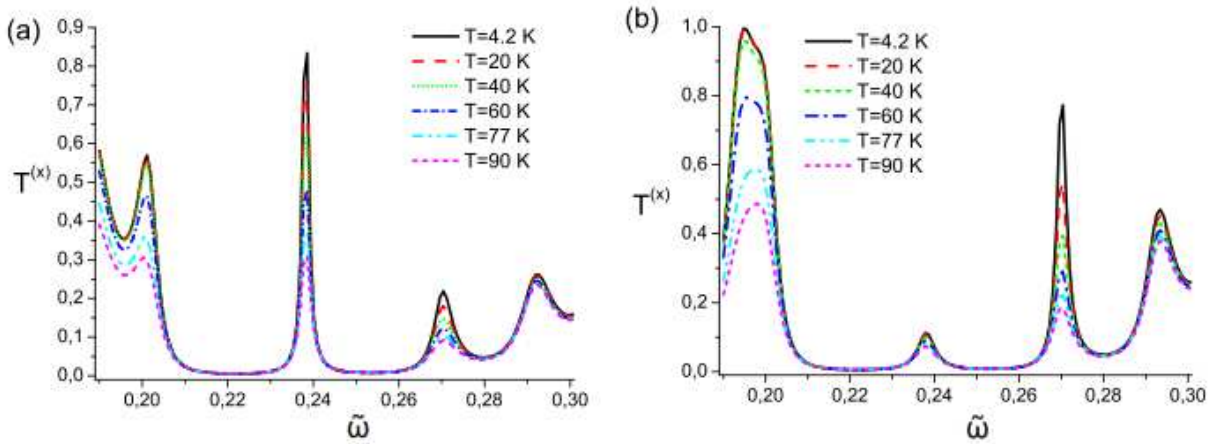


Figure 16. The temperature evolution of transmittivity spectra for the PC with RH – LH (a) and (b) LH – RH complex SC defects. The results are obtained for the defect layer thicknesses $d_s=10$ nm and $d_{1d}=d_{1l}=2.1$ μm .

For the case of RH – LH geometry (Fig. 16(a)) the temperature increase leads to the abrupt fall of the transmittivity value $T^{(x)}$ at the LF defect mode $\tilde{\omega}_{LF}=0.23855$ from $T_{LF}^{(x)}\approx 0.83$ at $T=4.2$ K to $T_{LF}^{(x)}\approx 0.31$ at $T=90$ K. As well, the HF DM peak diminishes with increasing temperature from

$T_{HF}^{(x)} \approx 0.31$ at $T=4.2$ K, to $T_{HF}^{(x)} \approx 0.09$ at $T=90$ K. In Fig. 16(a) one can see an essential lowering of the LF PBG edge in contrast to the HF PBG edge, which practically does not change with temperature. In the case of LH – RH geometry (Fig. 16(b)) the temperature effects substantially on the HF defect mode: its magnitude drops more than four times from $T_{HF}^{(x)} \approx 0.775$ at $T=4.2$ K to $T_{HF}^{(x)} \approx 0.187$ at $T=90$ K. The changing of the LF DM is not essential: at $T=4.2$ K the LF DM peak is quite small ($T_{LF}^{(x)} \approx 0.118$) and at $T=90$ K, it diminishes for 39% of this value and becomes $T_{LF}^{(x)} \approx 0.072$. At liquid helium temperature the transmittivity $T^{(x)}$ at the LF PBG edge is very high $T_{LF}^{(x)PBG} \approx 0.996$ and with the increase of temperature to T_C it becomes more than two times smaller. The lowering of the HF PBG edge with temperature is not so pronounced ($T_{HF}^{(x)PBG}$ for $T=90$ K is 19% lower than for $T=4.2$ K).

Our numerical results demonstrate that the PBG spectra of the y -polarized waves practically do not change when d_s is about several tens of nanometers, in contrast to the case of the x -polarized EMWs. The analogous result was obtained in our previous calculations for the PCs with two RH and two LH combined SC defects in the previous subsection. In Fig. 17 we show the top-view of the transmittivity $T^{(y)}$ of y -polarized EMW as function of normalized frequency $\tilde{\omega}$ and the SC defect sublayer thickness d_s for RH – LH geometry. The corresponding dependence for LH – RH geometry looks similarly. As one can see from Fig. 17, the positions of both DM peaks and both the positions and values of the PBG edges stay practically without changes with increase of d_s . The variation of the DM transmittivity with d_s is quite small for the y -polarized EMWs in comparison with the x -polarized ones.

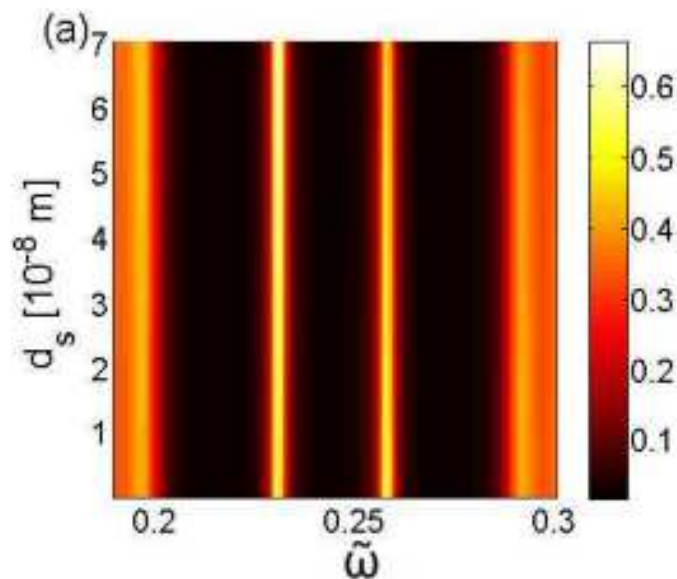


Figure 17. Top view of the transmittivities $T^{(y)}$ as function of $\tilde{\omega}$ and d_s (a). The results are obtained for the dielectric defect layer with $d_{1d}=2.1$ μm for $T=4.2$ K.

In contrast to the x -polarized EMWs, the spectra of the y -polarized EMWs practically do not exhibit noticeable modification with temperature for both (RH – LH and LH – RH) geometries. According to our estimations, for RH – LH geometry, the lowering of the transmittivities at frequencies of the LF DM and HF DM (with temperature increasing from $T=4.2$ K to $T=77$ K) is about 2% and 1.7% of their corresponding values for $T=4.2$ K, respectively. For the LH – RH geometry the lowering of DM peaks are 1.9 for the LF DM and 1.72% for the HF DM.

Above we investigated the PC with two combined defects (of RH – LH or LH – RH geometries) and supposed the equal thicknesses of the SC sublayers. Also we can fix one of the SC sublayer thicknesses d_{sR} or d_{sL} (in the left or right combined defect layer, respectively) and vary the other SC sublayer thickness, one can obtain a changing of the PBG spectra. Further we refer to this case, as an asymmetrical change of the SC defect sublayers. We start the investigation of the asymmetrical change of the SC defect sublayer thickness for the PC of RH – LH geometry. In Figs. 18(a) – 18(c) we present the top views of transmittivity $T^{(x)}$ of x -polarized EMWs as function of $\tilde{\omega}$ and d_{sR} with the fixed left-sided SC defect thicknesses $d_{sL}=10$ nm (a), $d_{sL}=20$ nm (b), and $d_{sL}=30$ nm (c). Comparing Figs. 15(a) and 19(a) – (c) for symmetrical and asymmetrical changes of the SC defect layers thickness, one can see, that the behavior of the DMs is changed. In contrast to the case of the equal thickness SC sublayers given in Fig. 15(a), for the case of fixed $d_{sL}=10$ nm both LF and HF DMs are practically do not change their positions with the increase of d_{sR} . Moreover, the HF DM is more broadened and it merges with the HF PBG edge completely for all d_{sR} for $d_{sL}=30$ nm (see Fig. 18(c)), so in this case we have only one DM inside the PBG. Comparing the transmittivity of the LF DM for the same values of d_{sR} at the Figs. 18(a) – (c), one can see that $T^{(x)}$ diminishes with the increase of d_{sL} .

Varying the left-sided SC defect layer thickness d_{sL} with fixed d_{sR} , one can obtain another behavior of the spectra with fixed thickness $d_{sR}=10, 20$ and 30 nm) are given in Figs. 18(d), 18(e), and 18(f), respectively. For this case a shift of both DMs to higher frequencies remains for $d_{sR}=10, 20$ and 30 nm, similar to the case of symmetric change of d_s which is shown in Fig. 15(a). But with the increase of the fixed value of d_{sR} to 20 nm the LH PBG edge peak sharpens and for $d_{sL}=30$ nm it splits of PBG transforming to the new pronounced DM, while the transmittivity of the HF DM as well as of the FH PBG edge, decreases with increasing of d_{sR} . In Fig. 18(f) both the new DM and the LF DM slightly deviate to higher frequencies with the increasing d_{sL} .

Analogously, in the case of the PC of the LH – RH geometry, the asymmetric changing of the SC defect sublayer thickness modifies the dependence of the transmittivity specter given in Fig. 15(b) for the symmetric changing of d_s . As one can see from Figs. 19(a) – 19(c), for the fixed values of d_{sL} , the LF PBG edge does not shift to higher frequencies with the increasing d_{sR} as in Fig. 15(b). The LF DM decreases fast with the increase of d_{sR} and d_{sL} .

Varying d_{sL} for the fixed values of d_{sR} , one cannot shift the LF DM to higher frequencies, as shown in Figs. 19(d) – (e), but the transmittivity of the LF DM decreases sharply with the increase of d_{sL} and it is practically suppressed for $d_{sR}=30$ nm. For $d_{sR}=30$ nm the HF DM merges with HF PBG edge for small values of d_{sL} .

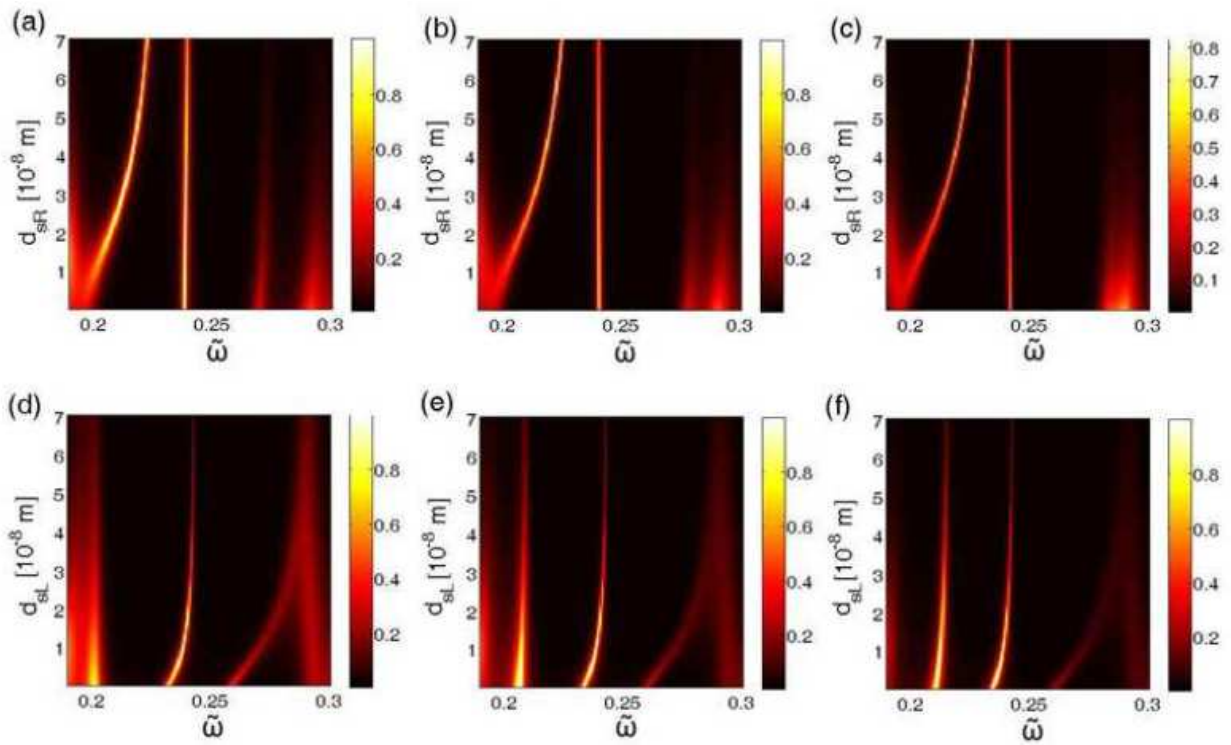


Figure 18. RH – LH geometry. Top view of the transmittivities $T^{(x)}$ vs $\tilde{\omega}$ and d_s for the case of fixed left-sided SC defect thickness: (a) $d_{sL}=10$ nm, (b) $d_{sL}=20$ nm, and (c) $d_{sL}=30$ nm ; and for the case of fixed right-sided SC defect thickness: (d) $d_{sR}=10$ nm, (e) $d_{sR}=20$ nm, and (f) $d_{sR}=30$ nm. The calculations are performed for $T=4.2$ K, $d_{id}=d_1$.

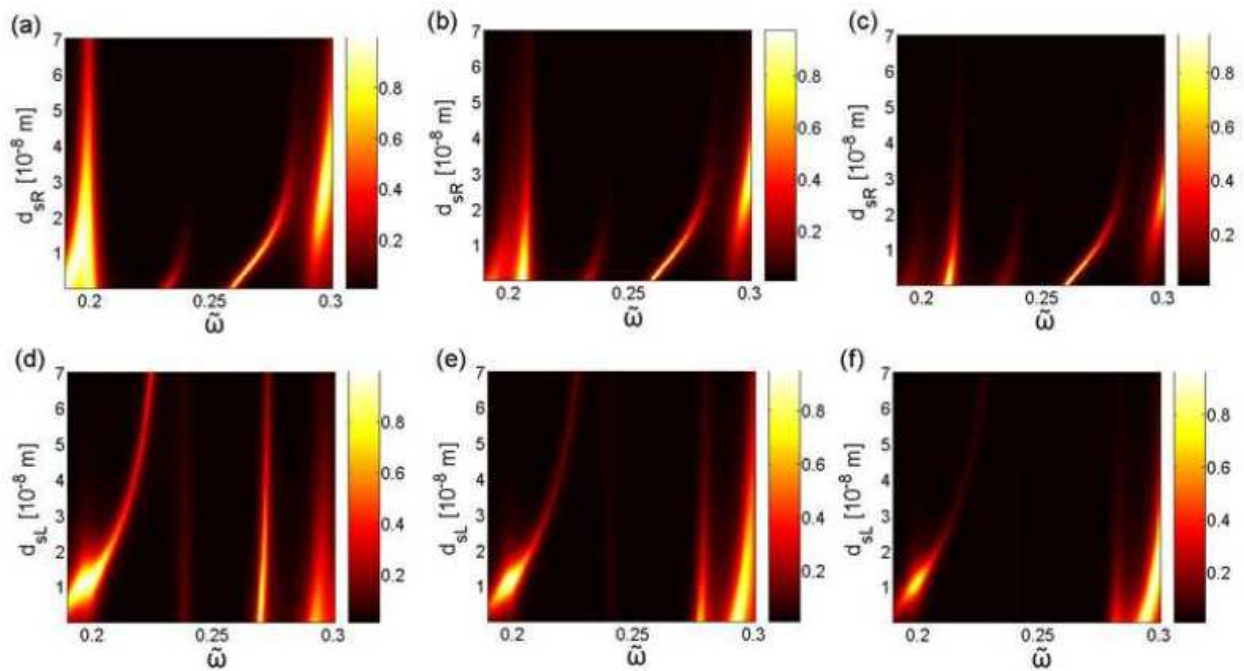


Figure 19. The same as for Fig. 9, except for LH – RH geometry.

4. Conclusions

In conclusion, we have investigated the behavior of DMs in a 1D dielectric PC with two complex bilayer defects composed of SC and dielectric constituents. We have considered the case of a fixed distance between the two defects embedded into the PC asymmetrically, i.e., when both SC sublayers are located on the right-hand side (RH – RH geometry) or on the left-hand side (LH – LH geometry) with respect to the dielectric parts of the complex defects. The normal incidence of linearly polarized EMWs (with electric field vector \mathbf{E} perpendicular to the axis of the PC's growth direction) on the PC is investigated.

The positions of the transmittivity peaks at the DM frequencies inside the first PBG are studied both analytically and numerically, for different temperatures and thicknesses of SC and dielectric sublayers. We have shown that the increase of temperature from liquid helium temperature ($T=4.2$ K) to the critical temperature of the SC sublayer ($T_c=90$ K for $YBa_2Cu_3O_7$) leads to significant changes of the DM's transmittivity peaks in the PBG spectra of x -polarized EMWs, up to a practically complete suppression of one of them (the low-frequency DM for RH – RH geometry), while the spectra of y -polarized EMWs are practically unchanged. The pronounced contrast in behavior of x - and y -polarized modes is based on the in-plane anisotropy of the dielectric tensor components of the SC sublayer. The positions of PBG edges and DM's remain invariable with temperature for both EMW's polarizations. We have demonstrated a high sensitivity of the PBG spectra of x -polarized EMWs to variations of the SC defect sublayers thicknesses in both RH – RH and LH – LH geometries. The increase of the SC defect sublayer thickness leads to a shift of both DM peaks towards the high-frequency PBG range up to their mergence with it, as well as to a decrease of the distance between these peaks (for RH – RH geometry), or a substantial shift of the position of the low-frequency PBG edge to higher frequencies (LH – LH geometry).

We have also considered the case of a fixed distance between the two defects symmetrically embedded into the PC, i.e., when one of the SC sublayers is located on the right-hand side and the another one on the left-hand side with respect to the dielectric parts of the complex defects (the cases of RH – LH and LH – RH geometries). The increase of the SC defect sublayer thickness leads to a shift of both DM peaks towards the high-frequency PBG range up to mergence of the one of them with it (in the RH – LH geometry), as well as to an increase of the distance between these peaks, or a substantial shift of the position of the low-frequency PBG edge to higher frequencies (in both RH – LH geometries). The variation of the dielectric defect sublayer's thicknesses allows shifting the DM peaks in spectra of both x - and y -polarized EMWs towards the low-frequency PBG edge for each geometry (RH – RH, LH – LH, RH – LH, and LH – RH).

Changing the SC defect sublayer thicknesses asymmetrically (when the right or the left SC defect sublayer's thickness is fixed while the another one is varied), one can modify the PBG spectra of x -polarized EMWs, changing the number of the defect modes in the PBG with chosen thicknesses of the SC defect sublayers.

As follows from our numerical results, the dielectric PCs with SC defects can be used as constituents of polarization-selective narrow-band filters for THz radiation [31, 32]. The

optimal parameters of these filters can be obtained choosing the proper SC and dielectric defect sublayer thicknesses. The high sensitivity to temperature of the PCs with SC defects opens possibilities to use such a structures as the basis of temperature tunable electromagnetic filters in the THz regime [33].

Author details

N. N. Dadoenkova^{1,2}, A. E. Zabolotin¹, Yu. S. Dadoenkova^{1,2}, I. L. Lyubchanskii^{1*}, Y.P. Lee³ and Th. Rasing⁴

*Address all correspondence to: igorl@fti.dn.ua

1 Donetsk Physical & Technical Institute of the National Academy of Sciences of Ukraine, Donetsk, Ukraine

2 Ulyanovsk State University, Ulyanovsk, Russian Federation

3 q-Psi and Department of Physics, Hanyang University, Seoul, Republic of Korea

4 Radboud University Nijmegen, Institute for Molecules and Materials, Nijmegen, The Netherlands

References

- [1] Yablonovich E. *Physical Review Letters* 1987; 58: 2059.
- [2] John S. *Physical Review Letters* 1987; 58: 2486.
- [3] Jannopoulos JD, Johnson SG, Winn JN, and Meade RD. *Photonic Crystals: Molding the Flow of Light*, 2nd ed. Princeton, New York: Princeton University Press; 2008.
- [4] Sakoda K. *Optical Properties of Photonic Crystals*. Berlin: Springer; 2005.
- [5] Vittorio M.N. Passaro., editor. *Advances in Photonic Crystals (Intechopen)*; 2013.
- [6] Shabanov VF, Vetrov SY, and Shabanov AV. *Optics of real photonic crystals. Mesomorphic Defects and Inhomogeneities*. Novosibirsk: Russian Academy of Sciences; 2005 (in Russian).
- [7] Lyubchanskii I L, Dadoenkova N N, Lyubchanskii M I, Shapovalov E A, and Rasing Th. *Journal of Physics D: Applied Physics* 2003; 36: R277.
- [8] Inoue M, Fujikawa R, Baryshev A, Khanikaev A, Lim P. B, Ushida H, Aktsipetrov O, Fedyanin A, Murzina T, and Granovsky A. *Journal of Physics D: Applied Physics* 2006; 39: R151.

- [9] Scott JF. *Ferroelectrics* 2003; 293: 33.
- [10] Fu Y, Zhang J, Hu X, and Gong Q. *Journal of Optics* 2010; 12: 075202.
- [11] Ferrini R. Liquid Crystals into Planar Photonic Crystals. In: Tkachenko GV. (ed.) *New Development in Liquid Crystals*. Rijeka: InTex; 2009. p21-48.
- [12] Da H-X and Li ZY. Manipulating Nematic Liquid Crystals-based Magnetophotonic Crystals. In: Tkachenko GV. (ed.) *New Development in Liquid Crystals*. Rijeka: InTex; 2009. p50-70.
- [13] Savel'ev S, Rakhmanov AL, and Nori F. *Physical Review Letters* 2005; 94: 157004.
- [14] Savel'ev S, Rakhmanov AL, and Nori F. *Physical Review B* 2006; 74: 184512.
- [15] Savel'ev S, Yampol'skii VA, Rakhmanov AL, and Nori F. *Repts. Progr. Phys.* 2010; 73: 026501.
- [16] Anlage SM. *Journal of Optics* 2011; 13: 024001.
- [17] Lyubchanskii IL, Dadoenkova NN, Zabolotin AE, Lee YP, and Rasing Th. *Journal of Optics A: Pure and Applied Optics* 2009; 11: 114014.
- [18] Dadoenkova NN, Zabolotin AE, Lyubchanskii IL, Lee YP, and Rasing Th. *Journal of Applied Physics* 2010; 108: 093117.
- [19] Rauh H and Genenko YA. *Journal of Physics of Condensed Matter* 2008; 20: 145203.
- [20] Barvestani J. *Optics Communications* 2011; 284: 231.
- [21] Bacerra G, Moncada-Villa OE, Granada JC. *Journal of Superconductivity and Novel Magnetism* 2012; 25: 2163.
- [22] Wu J, Gao J. *Holography, Proceedings of SPIE* 2012; 8556: 85561Q.
- [23] Hu C-A, Liu J-W, Wu C-J, Yang T-J, Yang S-L. *Solid State Communications* 2013; 157: 54.
- [24] Steel MJ, Levy M, and Osgood RM. *Journal of Lightwave Technology* 2000; 18: 1297.
- [25] Steel MJ, Levy M, and Osgood RM. *Journal of Lightwave Technology* 2001; 19: 1964.
- [26] Lyubchanskii IL, Dadoenkova NN, Lyubchanskii MI, Sapovalov EA, Zabolotin AE, Lee YP, Rasing Th. *Journal of Applied Physics* 2006; 100: 096110.
- [27] Lyubchanskii IL, Dadoenkova NN, Zabolotin AE, Lee YP, Rasing Th. *Journal of Applied Physics* 2008; 103: 07B321.
- [28] E. D. Palik. *Handbook of Optical Constants of Solids*. New York: Academic Press; 1991.
- [29] Berreman DW. *Journal of the Optical Society of America* 1972; 62: 502.

- [30] Borisov SB, Dadoenkova NN, and Lyubchanskii IL. *Optics and Spectroscopy* 1993; 74: 670.
- [31] Gennaro ED, Zannini C, Savo S, Andreone A, Masullo MR, Castaldi G, Gallina I and Galdi V. *New Journal of Physics* 2009; 11: 113022.
- [32] Raum M, Li J-S, and Padilla WJ. *Journal of Infrared, Millimeter, and Terahertz Waves* 2013; 34: 1.
- [33] Liu J-W, Chang T-W, Wu C-J. Filtering Properties of Photonic Crystal Dual-Channel Tunable Filter Containing Superconducting Defects. *Journal of Superconductivity and Novel Magnetism* 2014; 27: 67-72.

IntechOpen

